Hybridization and its impact on the ontogenetic allometry of skulls in macaques

Subtitle: Hybridization's impact on ontogenetic allometry

Tsuyoshi Ito[1,2,*], Ryosuke Kimura[3], Hikaru Wakamori[2,†], Mikiko Tanaka[2], Ayumi Tezuka[4], Atsushi J. Nagano[4,5], Yuzuru Hamada[2], Yoshi Kawamoto[2,6]

1. The Kyoto University Museum, Kyoto University, Sakyo, Kyoto 606-8501, Japan

2. Primate Research Institute, Kyoto University, Inuyama, Aichi 484-8506, Japan

3. Department of Human Biology and Anatomy, Graduate School of Medicine, University of the Ryukyus, Nishihara, Okinawa 903-0215, Japan

4. Faculty of Agriculture, Ryukoku University, Otsu, Shiga 520□2194, Japan

5. Institute for Advanced Biosciences, Keio University, Tsuruoka, Yamagata 997-0017, Japan

6. Faculty of Veterinary Science, Nippon Veterinary and Life Science University, Musashino, Tokyo 180-8602, Japan

* Correspondence: ito.tsuyoshi.3a@kyoto-u.ac.jp

† Present affiliation: Education and Public Relations Department, Tama Zoological Park, Tokyo Zoological Park Society, Hino, Japan

Author Contributions

TI, RK, YH, and YK conceived the research. TI, HW, and YK performed basic molecular experiments. AT and AJN conducted ddRAD library preparation. YK contributed samples and data. TI and MT assessed the dental eruption-cranial suture stage. TI analyzed the data and drafted the manuscript. All authors approved the final version of this manuscript.

Acknowledgments

We thank Hideyuki Ohsawa, Yoshiki Morimitsu, Yasuyuki Muroyama, Shingo Maekawa, Hideo Nigi, Harumi Torii, Shunji Goto, Tamaki Maruhashi, Naofumi Nakagawa, Jun Nakatani, Toshiki Tanaka, Sachiko Hayakawa, Aya Yamada, Shuhei Hayaishi, Hironori Seino, Kei Shirai, Mami Saeki, Shizuka Kawai, Ko Hagiwara, Katsuya Suzuki, Kunihiko Suzuki, Junya Uetsuki, Misao Okano, Tadanobu Okumura, Atsuhisa Yoshida, and Noriko Yokoyama, of the Working Group of Wakayama Taiwanese

macaque, and the Department of Environment and Life, Wakayama Prefecture, for kindly allowing us to use the samples. We also thank Yuta Shintaku and Takeshi Nishimura for their help in accessing the skeletal collections. We are grateful to Akira Kawaguchi, Kyoko Yamaguchi, Takehiro Sato, and Chikatoshi Sugimoto for teaching molecular experiments to TI. We express our gratitude to the successive members of the Department of Evolution and Phylogeny, Primate Research Institute, Kyoto University, for their efforts in collecting, preparing, and preserving skeletal collections. This study was funded by the Keihanshin Consortium for Fostering the Next Generation of Global Leaders in Research (K-CONNEX) established by the Human Resource Development Program for Science and Technology, MEXT, JSPS KAKENHI (Grant Numbers: JP15J00134, JP17K15195, JP19K16211, and JP19H01002), the University of the Ryukyus Research Project Program Grant for Junior Researchers, the Cooperative Research Program from the Primate Research Institute of Kyoto University, and ISHIZUE 2022 of Kyoto University o TI.

Data Accessibility Statement

The sequence reads have been submitted to the Sequence Read Archive (SRA) of the National Center for Biotechnology Information (NCBI) under accession number PRJNA1009132. The other data underlying this article are available in the Dryad Digital Repository, at https://doi.org/10.5061/dryad.d2547d87h. (These data will be available upon acceptance of this article.)

Conflicts of interest

The authors declare no conflicts of interest.

Hybridization and its impact on the ontogenetic allometry of skulls in macaques

Abstract

The importance of hybridization in morphological diversification is a fundamental topic in evolutionary biology. However, despite accumulated knowledge concerning adult hybrid variations, how hybridization affects ontogenetic allometry is less well understood. Herein, we assessed the effects of hybridization on the postnatal ontogenetic allometry in skulls of a putative hybrid population of introduced Taiwanese macaques (*Macaca cyclopis*) and native Japanese macaques (*M. fuscata*). Genomic analyses indicated that the population consisted of individuals with various degrees of admixture, formed by male migration of Japanese to Taiwanese macaques. No marked ontogenetic trajectory angle dissociation was observed in the overall skull shape of hybrids. Transgressive variations in the overall skull shape were observed mainly in non-allometric components. Hybridization collapsed a mechanism found in Japanese macaques that restricts the growth rate of the maxillary sinus (the hollow space in the face), producing hybrids with a mosaic pattern, i.e., the maxillary sinus is as large as that in Taiwanese macaques, although the overall skull shape is intermediate. Our findings suggest that the transgressive variations can be caused by prenatal shape modifications and the lifting of the genetic restriction on the regional growth rate, highlighting the complex genetic and ontogenetic bases underlying hybridization-induced morphological diversification.

Keywords: allometry, hybridization, geometric morphometrics, paranasal sinus, ontogeny, population genomics

1. Introduction

Growing understanding indicates that interspecific hybridization is not rare, even in animals (Mallet 2005; Taylor and Larson 2019). Furthermore, hybridization is not always maladaptive and can facilitate evolutionary novelty and diversity by generating gene combinations not achieved in parental lineages (Seehausen 2004; Arnold and Kunte 2017; Kagawa and Takimoto 2018). Thus, hybridization must have played a critical role in the evolution of various taxa and has consequently been of significant interest to evolutionary biologists.

Primate hybridization is of particular interest as this improves comprehension of the effects of archaic human gene introgression on the modern human lineage. Molecular studies show that hybridization is pervasive in primates, with relics of ancient hybridization or the existence of a natural hybrid zone identified in various taxa of primates, e.g., macaques, baboons, vervet monkeys, marmosets, colobine monkeys, and howler monkeys (Roos et al. 2011; Malukiewicz et al. 2014; Cortés-Ortiz et al. 2015; Svardal et al. 2017; Rogers et al. 2019; Osada et al. 2021). Furthermore, several studies have assessed the morphological effects of hybridization in nonhuman primates (Ackermann et al. 2019). In baboons and gorillas, hybrids exhibit anomalies such as supplementary rotated teeth or atypical sutures of the cranium at higher frequencies than are present in their parental lineages (Ackermann and Bishop 2010; Ackermann et al. 2014). In various taxa of primates, hybrids often show heterotic/transgressive phenotypes or increased variation in cranial and postcranial morphologies (Cheverud et al. 1993; Ackermann et al. 2014; Fuzessy et al. 2014; Ito et al. 2015; Eichel and Ackermann 2016; Boel et al. 2019; but see Buck et al. 2021). Such hybridization-driven genetic perturbations may contribute to the morphological diversity in primate evolution.

Any morphological evolution is achieved by the dissociations of the ancient ontogenetic trajectory. For example, a distinct adult human craniofacial morphology is formed by the divergence from the hominid common ontogenetic trajectory in the early postnatal period (Mitteroecker et al. 2004). The difference in brain (endocast) shape between modern humans and Neanderthals was also formed by the early divergence (Gunz et al. 2010); however, the overall craniofacial difference between the two species was formed by a more or less parallel (but not identical) ontogenetic trajectory originating from the established difference at birth (Ponce de León and Zollikofer 2001; Bastir et al. 2007). As the ontogenetic trajectory reflects the expression of genes that control morphology during development, hybridization-induced genomic admixture potentially alters an ontogenetic trajectory. Hybrid Sulawesi macaques are reported to show acceleration (slope increase) and postdisplacement (intercept decrease) in the ontogenetic trajectory of several craniofacial traits, although this dissociation does not account for adult heterosis (Schillaci et al. 2005). Predisplacement (intercept increase) occurs in the ontogenetic trajectory of body weight of inter-subspecies male hybrids of rhesus macaques but is lacking in female hybrids (Smith and Scott 1989; Taylor and Schillaci 2008). In non-primate taxa, several studies detected various types of ontogenetic modifications, e.g., pure heterochrony, direction dissociations, or intermediate but maternally biased trajectory, in the head or body shape of fish hybrids (Holtmeier 2001; Corse et al. 2012; Sinama et al. 2013; Santos-Santos et al. 2021). However, with the exception of these studies, there remains limited knowledge concerning the effects of interspecific hybridization on an ontogenetic trajectory, especially in mammals.

Anthropogenic hybridization provides opportunities to examine the consequences of hybridization, although it is controversial in the context of conservation. In the Oike area of Wakayama Prefecture, Japan, introduced *Macaca cyclopis* (Taiwanese macaques) that escaped from a zoo in

the 1950s hybridized with native *M. fuscata* (Japanese macaques) (Ohsawa et al. 2005). By 2004, the population had grown to approximately 300 with four troops (Ohsawa et al. 2005). Genetic analyses suggested that the Oike hybrid population was formed by male immigration from the neighboring native population of *M. fuscata* into *M. cyclopis* (Kawamoto et al. 2001, 2008a). The government began the elimination of introduced and hybrid individuals from the Oike area to prevent genetic introgression and its impacts on ecosystems in 2002 and finally declared eradication in 2017, with 366 individuals eradicated from the Oike area in total (Shirai et al. 2018). The Oike hybrids show several intriguing morphological variations. For example, unlike the previous studies targeting hybrids of other primate taxa, the Oike hybrids lacked a marked increase in dental anomalies or craniofacial variability compared with their parental species (Boel et al. 2019). The relative tail length variations followed additive model expectations (Hamada et al. 2012). The overall craniofacial shape in adults also follows the additive model expectation or was somewhat closer to that of *M. fuscata* than expected; by contrast, the maxillary sinus size (hollow space in the face) was much closer to that of *M. cyclopis* than the additive model expectation (Ito et al. 2015; Boel et al. 2019). However, it remains unclear how these adult variations manifested during development.

This study sought to elucidate the effects of hybridization on the ontogenetic trajectory of craniofacial morphology using the samples of the Oike hybrid population. First, we estimated the population structure of the Oike population as well as the hybrid index and class (generation) of individuals based on the genome-wide single nucleotide polymorphisms (SNPs). Second, we compared the morphological variations and ontogenetic trajectories of the cranium, mandible, and maxillary sinus with the hybrid index and among the hybrid classes. Comparing the ontogenetic

trajectories among hybrids and parental lines will increase our understanding of genetic and ontogenetic bases of hybridization-induced morphological diversification.

2. Materials and methods

2.1. Samples

Almost all available samples of the Oike hybrid population were screened, including 245 skeletal specimens and 287 DNA samples (Table S1; Fig. 1). Note that some samples were filtered out before the main analyses (see below for details). Of these, the 215 skeletal specimens could be linked to DNA samples, where we linked them as far as IDs on records were uniquely identified even if they did not show exact matching. These samples were provided from collections obtained under the government eradication program between 2003 to 2006; no animals were sacrificed for research purposes. Skeletal specimens are stored at the Primate Research Institute (now the Center for the Evolutionary Origins of Human Behavior), Kyoto University (Inuyama, Japan). Note, any individuals judged as pure Japanese macaques in the Oike area had been released (Hamada et al. 2008).

Additionally, to check whether pure parental individuals remained in the Oike population, we examined the DNA from pure captive *M. cyclopis* (N = 4) and *M. fuscata* (N = 4) housed at the Primate Research Institute. The *M. fuscata* individuals were descendants of those transferred from Arashiyama, Kyoto, approximately 100 km north-northeast of the Oike area. The *M. cyclopis* individuals have no record of their exact origin. Sample collection from these captive individuals was performed according to recommendations in the Guidelines for Care and Use of Nonhuman Primates Version 2 and 3 of the Primate Research Institute, Kyoto University (2002, 2010). DNA was extracted from blood using the phenol–chloroform method.

Skeletal specimens of *M. cyclopis* (*N* = 54) and *M. fuscata* (*N* = 88) stored at the Primate Research Institute and the Japan Monkey Centre (Inuyama, Japan) were assessed as a surrogate for parental individuals for morphological analyses (because actual parental populations are unknown). Captive and unknown-origin specimens were initially included; however, preliminary analyses detected wild-captive morphological differences (see below). Thus, only wild specimens (*N* = 18 for *M. cyclopis*, *N* = 86 for *M. fuscata*) were used for the main analyses. Wild *M. cyclopis* specimens were obtained from the introduced population in Izu-Oshima Island, Tokyo, Japan, where *M. fuscata* is not distributed. Wild *M. fuscata* specimens were obtained from localities around the Oike area, and are therefore likely to be genetically close to a parental population (Suzuki-Hashido et al. 2015; Ito et al. 2021).

2.2. Double-digest restriction site-associated DNA library preparation and sequencing

Double-digest restriction site-associated DNA sequencing was performed based on Peterson's protocol (Peterson et al. 2012) with modifications (Sakaguchi et al. 2015, 2017). Genomic DNA (10 ng) was digested with EcoRI and BglII (New England Biolabs, Ipswich, MA, USA), and adapters were ligated at 37 °C overnight in a 10-μL volume containing 1 μL of ×10 NEB buffer 2, 0.1 μL of ×100 bovine serum albumin (New England Biolabs), 0.4 μL of 5 μM EcoRI adapter and BglII adapter, 0.1 μL of 100 mM ATP and 0.5 μL of T4 DNA Ligase (Enzymatics, Beverly, MA, USA). The reaction solution was purified with AMPure XP (Beckman Coulter). Next, 3 μL of purified DNA was used in the PCR amplification in a 10-μL volume containing 1 μL of each 10 μM index and TruSeq universal primer, 0.3 μL of KOD-Plus-Neo enzyme, and 1 μL of ×10 PCR buffer (Toyobo, Osaka, Japan), 0.6 μL of 25 mM MgSO4 and 1 μL of 10 mM dNTP. Thermal cycling was initiated with a 94 °C step for 2 min, followed by 20 cycles of 98 °C for 10 s, 65 °C for 30 s, and 68 °C for 30 s. PCR products were pooled and purified again with AMPure XP. Purified

DNA was loaded onto a 2.0% agarose gel, and fragments of around 360 base pairs (bp) were retrieved using E-Gel SizeSelect (Life Technologies, Carlsbad, CA, USA). After quality assessment using an Agilent 2100 Bioanalyzer (Agilent Technologies, Santa Clara, CA, USA), the library was sequenced with 51-bp single-end reads in six lanes of an Illumina HiSeq2000 (Illumina, San Diego, CA, USA) by Macrogen Inc. (Seoul, South Korea). Primer sequences used in this study are available in Sakaguchi et al. (2015).

2.3. Variant calling and filtering

Raw reads were filtered for overall sequence quality using TRIMMOMATIC 0.39 (Bolger et al. 2014) with the following parameters: ILLUMINACLIP:TruSeq3-SE.fa:2:30:10, LEADING:19, TRAILING:19, SLIDINGWINDOW:30:20, and AVGQUAL:20 MINLEN:51. Filtered reads were mapped to the RefSeq of *M. mulatta* (rhesus macaque) (Mmul_10; GCF_003339765.1) using BOWTIE2 2.4.4 (Langmead and Salzberg 2012) with –very-sensitive option. The sex of each individual was assessed based on the ratio of the number of reads mapped onto the Y-chromosome versus those mapped to the X-chromosome, using sam_sexing.py (https://github.com/itots/sam_sexing.git). Genotypes were called using STACKS 2.59 (Rochette and Catchen 2017), wherein the Marukilow model in the gstacks function was applied to search variant sites with relatively stricter criteria than the default setting: –var-alpha 0.01 (a significant level for calling variant sites), –gt-alpha 0.01 (a significant level for calling genotype), and –min-mapq 20 (minimum PHRED-scaled mapping quality to consider a read). Next, the populations function was used for calling SNPs with the following parameters: –write-single-snp (extract only the first SNP per locus) and –ordered-export. Since STACKS provides diploid genotypes, those on the sex chromosomes of males were converted to be haploid using

diploid2haploid.py (https://github.com/itots/diploid2haploid.git), where heterogeneous genotypes (1.2% for X-chromosome and 0.8% for Y-chromosome) were omitted.

The SNPs dataset was filtered using PLINK 1.90b6.21 (Purcell et al. 2007; https://www.cog-genomics.org/plink2/) to retain individuals with missing rate <0.2 and sites with missing rate <0.2 and minor allele frequency >0.01 (–geno 0.2 –mind 0.2 –maf 0.01). Autosomal and X-chromosome SNPs were further filtered to remove sites in strong linkage disequilibrium (–indep-pairwise 10 3 0.5). These filtrations yielded 6461 variant sites in 289 individuals for autosome (total genotyping rate = 0.96), 171 sites in 289 individuals for X-chromosome (0.96), and 12 sites in 152 individuals for Y-chromosome (0.95) DNA.

2.4. Global ancestry inference and data screening

Global ancestry was inferred based on the SNPs separately for autosomes and X-chromosomes, using ADMIXTURE (Alexander and Novembre 2009); the X-chromosome of males were treated as haploid using the –haploid flag. Principal component analysis (PCA) was performed using the "adegenet" package (Jombart 2008) in R (R Developmental Core Team 2021). For Y-chromosome, the *K*-means cluster analysis ($K = 2$) was performed based on the first principal component (PC).

Data were also examined from Kawamoto et al. (2008a), including sex, and a nine-step hybrid index calculated from four autosomal markers (blood proteins of transferrin, adenosine deaminase, diaphorase, and SNP of natural resistance-associated macrophage protein 1), and ancestry types of the mitochondrial DNA (mtDNA) and the testis-specific protein Y (TSPY). Some missing data on the Y-chromosome ($N = 52$) and mtDNA ancestries ($N = 9$) were supplemented in this study; the method applied was identical to that in Kawamoto et al. (2008a), but if the results of the TSPY

marker were unclear, two STR markers (DYS472 and DYS569) were additionally examined following Kawamoto et al. (2008b).

To screen the data, data from Kawamoto et al. (2008a) and this study were compared. Sex identification was inconsistent in five samples. The ADMIXTURE Q score (K = 2) was highly correlated with the nine-step hybrid index (R^2 = 0.79, $F_{1, 275}$ = 1005.7, P < 0.001), but two samples were detected as outliers in their residual component (Bonferroni-adjusted P < 0.05). These six samples (one sample showed inconsistency in both tests) were removed from the analyses. The Y-chromosome ancestry was identical between the two datasets, except for three samples with missing values in Kawamoto et al. (2008a).

2.5. Hybrid index and class

Individuals in the Oike population were classified into 23 *M. cyclopis* (Q < 0.001), 11 *M. fuscata* (Q > 0.999), and 242 putatively admixed individuals (0.001 ≤ Q ≤ 0.999) based on the ADMIXTURE Q score (K = 2) of autosomal SNPs. Diagnostic markers were detected as differentially fixed sites (allele frequency difference between the two parental populations [δ] = 1), wherein loci with missing genotype rates within any of the two parental populations > 0.1 were omitted. Hybrid index, the proportion of the ancestry belonging to *M. fuscata*, and interspecific heterozygosity, the proportion of loci with alleles from both parental populations, were calculated based on the 196 autosomal diagnostic markers using a custom R script.

The hybrid class was estimated for individuals of the Oike population using NewHybrids 1.1 (Anderson and Thompson 2002). This Bayesian-based method calculates the posterior probability that an individual belongs to a genotype frequency class. The SNP dataset of 196 autosomal diagnostic markers was converted to a NewHybrid format using PGDSpider 2.1.1.5 (Lischer and

Excoffier 2012). The “z” option was applied to instruct NewHybrid that the individuals with a hybrid index = 0 or 1 were pure parental individuals. Ten replicates were run with randomly differentiating seeds using the “parallelnewhybrid” R package (Wringe et al. 2017) with minor modifications (https://github.com/itots/parallelnewhybrid.git). Each run started with Jeffery’s prior and default six genotype frequency classes and consisted of 10,000 Markov Chain Monte Carlo (MCMC) sweeps after 10,000 burn-in iterations. We confirmed MCMC convergence by visual inspection. Based on the mean posterior probabilities, each individual was assigned to one of six genealogical classes: *M. cyclopis* (P0), *M. fuscata* (P1), F1, F2 hybrids, and backcrosses of *M. cyclopis* (BC0) and *M. fuscata* (BC1). We discarded assignments with mean posterior probability <0.99, P0 with hybrid index >0, P1 with hybrid index <1, and F1 with interspecific heterozygosity <0.95; these were removed from the analyses that evaluate hybrid class differences (represented as NA in figures). Note that individuals identified as F2, BC0, and BC1 may include later generations; unfortunately, it is difficult to distinguish between the hybrid classes of recombinant generations based on unphased and limited numbers of variants.

2.6. Morphological data collection and screening

The 10-step dental eruption-cranial suture stage was determined based on the dental eruption pattern and spheno-occipital synchondrosis, according to Mouri (1994), with minor modifications (Table S2). Based on this, developmental stages were determined as infants (dental eruption-cranial suture stage <3), juveniles (<8), and adults (≥8). These stages were used to evaluate age structure and developmental changes in morphology.

Craniums and mandibles were assessed with computed tomography (CT), the Asteion Premium 4 helical scanner (Toshiba Medical Systems, Otawara, Japan), with a 0.5-mm thick slice at the

Primate Research Institute. Serial CT images were reconstructed from original volumetric data, with a pixel size between 0.093 to 0.314 mm and an inter-slice interval between 0.1 to 0.3 mm, depending on the specimen size. CT images were segmented based on edge detection and watershed methods (Ito 2019), and three-dimensional (3D) surface models were created using the Python (create_mesh.py; https://github.com/itots/dicom2stl.git).

Image stacks and the 3D models were loaded into 3D Slicer (https://www.slicer.org/) (Kikinis et al. 2014), and 3D landmarks were digitized on the cranium (the number of landmarks = 50), the mandible (28), and maxillary sinus (10) (Table S3; Fig. 2). All landmarks on the maxillary sinus were Type III and were used only to evaluate the size, not shape. Digitization was performed twice for all the specimens by a single observer to evaluate and minimize measurement errors. Samples with a missing landmark ratio > 0.2 (three samples for the cranium and one for the mandible) were removed. For the remaining samples, missing landmarks (1–10 in 53 samples for the cranium, 1–4 in 10 samples for the mandible, and 1–2 in 30 samples for the maxillary sinus) were imputed based on the Bayesian PCA method, using the “LOST” R package (Arbour and Brown 2014, 2020).

The generalized Procrustes analysis and Procrustes analysis of variance were performed to evaluate measurement errors using the “geomorph” R package (Collyer and Adams 2018, 2021; Adams et al. 2021; Baken et al. 2021). Here, the centroid size was calculated as the square root of the sum of squared distances of a set of landmarks from their centroid. For the cranium and mandible, measurement errors of shape were negligible compared with inter-individual variations (Table S4), and a symmetric component was used in the following analyses. Measurement errors were negligible in the centroid size of the cranium, mandible, and maxillary sinus (Table S5), and the mean of replicates (mean of replicates and sides for maxillary sinus) was used in the following analyses.

Only wild specimens were analyzed because significant morphological differences were detected between captive and wild samples (Tables S6 and S7). Samples with missing values for sex (*N* = 1–2), hybrid index (*N* = 28), and hybrid class (*N* = 40–41) were excluded from the subsequent analyses and figures requiring these variables.

2.7. Statistical analyses of morphological data

To evaluate the effect of hybridization on growth trajectories, the natural logarithm of the centroid size (lnCS) was evaluated in relation to the dental eruption-cranial suture stage for each hybrid class. To summarize the shape variation of the cranium and mandible, PCA was performed on the shape components, with all samples pooled, using the "geomorph" R package, but each sex was shown separately in the scatterplots for better visibility. Differences in lnCS and PCs between hybrid classes at each stage were evaluated by analysis of variance with sex as a covariate using the "car" R package (Fox and Weisberg 2019), and their effect sizes were evaluated using the "rstatix" R package (Kassambara 2023).

Ontogenetic shape allometry was evaluated by a multivariate regression using the "geomorph" R package. The response variable was the shape component, and the explanatory variables were lnCS, hybrid class, and their interaction. Pairwise vector correlations were evaluated using the "RRPP" R package (Collyer and Adams 2018, 2021). Phenotypic trajectory analysis was also performed to evaluate the trajectory magnitude, direction, and shape differences among the hybrid classes, using the "geomorph" R package. Here, developmental stage, hybrid class, and their interaction were used as the explanatory variables; a hybrid class lacking any of the three developmental stages was omitted. For the maxillary sinus, reduced major axis regression was

performed to assess the relationship between sinus lnCS and cranial lnCS, and slope and elevation differences among hybrid classes were tested using the "smatr" R package (Warton et al. 2012).

Variations in adults were evaluated in relation to the hybrid index. To detect shape differences between pure *M. cyclopis* and *M. fuscata*, between-group PCA (bgPCA) was performed, and admixed individuals were projected onto the bgPC1 axis, using the “Morpho” R package (Schlager 2017). The lnCS, bgPC1, and the relative sinus size (sinus lnCS – cranium lnCS) were regressed against the hybrid index for the admixed individuals, and the deviations in elevation and slope from the additivity (the line passing through the means of each parent) were tested, using the “smatr” R package.

Deviations from additivity in multivariate space were evaluated as two orthogonal components, mismatch (M) and bias (B):

$$M = \frac{d_{\mathrm{h}} \sin \theta}{d_{\mathrm{p}}},$$

$$B = \frac{d_{\mathrm{h}} \cos \theta}{d_{\mathrm{p}}},$$

where θ is the angle between the vector passing through the means of pure *M. cyclopis* and a hybrid class and that of pure *M. cyclopis* and *M. fuscata*; d_{h} and d_{p} are the magnitudes of the two vectors, respectively. For the shape of the cranium and mandible, distances were calculated as the Procrustes distance using the “shapes” R package (Dryden 2021). For the relative maxillary sinus size, only the closeness was calculated, as this is univariate. Females and males were separately analyzed. The M and B are similar to the transgression and closeness presented by Renaud et al. (2012), but differ in their orthogonality and are identical to the indices presented by Mérot et al. (2020) and Thompson et al. (2021) except for standardization. $M > 0$ indicates orthogonal deviations from the inter-parental axis, standardized by the inter-parental species distance. This is

caused by different traits having dominance in conflicting directions in multivariate space (Thompson et al. 2021). Any deviations of *B* from the hybrid index denote biases from additivity along the inter-parental axis, and particularly $B < 0$ and $B > 1$ indicate exceeding of parental means, i.e., over-dominance. *M* and *B* were calculated using a custom R script.

Each sex was analyzed separately in these analyses, unless otherwise noted.

3. Results

3.1. Population structure

PCA and ADMIXTURE showed that the Oike population consisted of individuals with various degrees of admixture, probably including pure *M. cyclopis* and *M. fuscata* (Figs. S1 and S2). The *M. cyclopis* individuals housed at the Primate Research Institute appeared to have a small portion of *M. fuscata*-derived ancestry (Fig. S2), but this did not affect the following analyses that included only the Oike population samples. The NewHybrids analysis indicated that the Oike population consists of the six predefined hybrid classes (P0, P1, F1, F2, BC0, and BC1; Fig. 3). It should be noted, however, that some of the individuals identified as F2, BC0, and BC1 might be from later generations. In the Oike population, the mean admixture proportion of *M. fuscata*-derived ancestry is 0.45 for autosomal, 0.46 for X-chromosomal in both sex, and 0.50 for Y-chromosomal DNA. Note that the mean admixture proportion for autosomes was slightly biased toward *M. cyclopis* in BC0 and F2 than expected by random mating starting from the same number of parental lines (Table S8). The *M. fuscata*-type mtDNA ancestry was observed only in the P0, namely pure *M. fuscata*. The P0 individuals were all males, while males were significantly less abundant than females in the F1 ($\chi^2 = 5.76, Df = 1, P = 0.016$) (Table S9; Fig. 3). In the

other hybrid classes, the sex ratios lacked any significant bias. The age structure was biased toward adults in F1 but was biased toward earlier stages in F2 (Table S10; Fig. 3).

3.2. Ontogenetic allometry

Throughout development, cranial and mandibular lnCS were larger in *M. fuscata* than in *M. cyclopis*, with hybrids in between in an almost additive manner (Table S11; Fig. S3). Among the first three PCs explaining >80% of the total variance, PC1 represented the ontogenetic allometric changes (Figs. 4 and S4), showing that larger (more developed) individuals had more elongated faces, relatively smaller neuro-craniums, and narrower and longer mandibles. A similar shape change was observed in the multivariate regression analysis (see below). In contrast, PC2 represented the interspecific differences throughout the development (Table S11; Figs. 4, S4 and S5). *M. fuscata* showed a relatively longer face with an inferiorly-inclined anterior maxilla and a mandible with a deeper ramus and shorter corpus than those of *M. cyclopis*; the hybrids were positioned in between in an almost additive manner.

The multivariate regression indicated that the allometric slope heterogeneity was small but marginally significant in the female mandible and male cranium (Tables 1 and 2; Figs. 5 and S6). The allometric elevations were significantly different among the hybrid classes, where the hybrids were positioned between the parental species. The allometric elevations were slightly biased toward *M. fuscata* in males than expected in the additive model, although the mean admixture proportion of autosomes was rather biased toward *M. cyclopis* in BC0 and F2 (Table S8). Phenotypic trajectory analysis supported the finding that the ontogenetic trajectories did not differ greatly in magnitude, direction, and shape among the hybrid classes, although in some cases they

were marginally significant (Table S12; Fig. 6). Several trajectories produced polygonal curves with detouring in juveniles and returning to an infant-like shape in adults.

The allometric slope of the maxillary sinus size significantly differed among the hybrid classes (Table S13; Fig. 7). Small, but significant, differences were present in the absolute and relative sizes of the maxillary sinus, even at the early dental stages (Table S11; Fig. S3). *M. fuscata* exhibited a gentler allometric slope than that in the other hybrid classes, including *M. cyclops*, and the difference between *M. fuscata* and the others, therefore, increased at later dental stages.

3.3. Adult morphology

The admixed adult individuals of the Oike populations followed additive model expectations or were sometimes slightly biased toward *M. fuscata* in the size and the shape component representing interspecific differences (bgPC1) (Table 3, S18; Fig. 8). Differences in the major allometric components (the PC1 and the regression score) among the hybrid classes were relatively small, although significant for the cranium PC1 at the dental eruption-cranial suture stage 10 (Tables S13 and S14; Figs. 4, 5, and S6). In contrast, the maxillary sinuses of the hybrids were as large as those of *M. cyclopis* regardless of the hybrid index and significantly deviated from the additive model expectations (Table S19; Fig. 8).

Marked transgressive segregations were observed in the shape of cranium and mandible (Table 4), particularly in the non-allometric shape space represented by PC2 and PC3 (Fig. S5). For cranial and mandibular shape, deviations from additivity were relatively small in the bias component, while the degree of mismatch was comparable to half the interspecific distance. Some hybrids were also transgressive in the morpho-space of cranium shape representing interspecific difference (PC2) and the relative size of the maxillary sinus (Fig. S7).

4. Discussion

4.1. Population structure

This study examined 281 samples (after filtering) captured between 2003 to 2006 in the Oike area. Considering that the estimated population size was approximately 200–300 in the early 2000s (Ohsawa et al. 2005) and that the total number of captured individuals was 366, the samples used in this study were sufficient to evaluate the population structure of the Oike area.

Our results suggested that the Oike population consisted of pure *M. cyclopis*, pure *M. fuscata* (only males), the first- and subsequent-generation hybrids, and the backcross hybrids of both parental species. The first generation mainly consisted of adults, whereas few adults were observed in the subsequent generations. This implies successful interbreeding between pure *M. cyclopis* and *M. fuscata* was likely sporadic and rare, at least in the years before eradication. In contrast, backcrossing and inter-hybrid breeding were probably pervasive. As indicated in previous studies (Kawamoto et al. 2001, 2008a), no *M. fuscata*-type mtDNA was observed in the admixed individuals, indicating that only male *M. fuscata* individuals migrated into the Oike population. Considering the philopatric nature of female macaques, this is a reasonable scenario. Given male migration and assuming random breeding, the proportion of the Y-chromosome ancestry was expected to be twice that of autosomes, but this was much lower than expected. Therefore, a mechanism that prevents random breeding, such as Haldane's rule, population subdivision, or assortative mating, may have existed in this population. Fewer males than females in the F1 generation imply a lower survival rate or emigration of males, although this is inconclusive because of the small sample size. The population subdivision scenario is also plausible, as four troops were observed in the Oike area (Ohsawa et al. 2005); heterogeneity in the migration rate

from neighboring *M. fuscata* among troops may underlie the relatively low frequency of *M. fuscat*a-type Y chromosome in the Oike population.

4.2. Effects of hybridization on the ontogenetic trajectory and adult morphology

In the multivariate shape space, the ontogenetic trajectories of the cranium and mandible were differentiated in elevation between the parental species. Hybridization shifts the ontogenetic trajectories by the proportion of ancestry, although this is in some cases slightly biased toward *M. fuscata* from that in the additive model expectations. No marked evidence of ontogenetic direction change was observed. In other words, the hybridization-induced shape differentiations were already manifested at birth; the differences are maintained during postnatal ontogeny. This result is consistent with those from a study of Sulawesi macaques that showed no marked differentiation in the ontogenetic trajectory of the cranium between hybrids and their parental species in multivariate allometric space (Schillaci et al. 2005). Schillaci et al. (2005) reported hybridization-induced heterochrony in several cranial traits in bivariate allometric trajectories; this is pure heterochrony (*sensu* Mitteroecker et al. 2004), which cannot be evaluated when trajectories do not overlap in multivariate space. Thus, hybridization did not alter the ontogenetic direction in the shapes of the cranium or mandible of the macaques but shifted the trajectory. The shifts in the major allometric component did not influence the variations in adult shape among the hybrids and their parental species. Instead, the hybridization-induced adult shape variations, including transgressive ones, were likely mostly caused by prenatal shape alternations.

It should be noted that the present finding of limited effects of hybridization on the direction of postnatal ontogenetic trajectory may be limited to the case of parental pairs showing parallel shift. The parallel ontogenetic trajectory differentiation among species has been widely observed in primate skull shape (Mouri 1996; Ponce de León and Zollikofer 2001; Toyoda et al. 2022), while

recent multivariate studies have shown that the direction of ontogenetic trajectories of cranial shape differs among species in some primate taxa (Mitteroecker et al. 2004; Vioarsdóttir and Cobb 2004; Singleton 2012; Simons and Frost 2021). How hybridization between species that show directional dissociation of ontogenetic trajectories affects ontogenetic direction is of interest for future studies.

The finding that transgressive segregation is observed in hybrids is consistent with many previous studies examining hybrid phenotypic variation in various taxa of organisms (Rieseberg et al. 1999; Albertson and Kocher 2005; Stelkens et al. 2009; Renaud et al. 2012; Ackermann et al. 2019). What our finding can add to the literature is that transgressive segregation is likely to manifest prenatally without much change postnatally. Transgressive segregation is often found in a trait composed of multiple modules, such as the cranium and mandible examined in our study, and is probably caused by different modules responding to hybridization in opposite directions (Albertson and Kocher 2005; Renaud et al. 2012). Whether and how transgressive segregation manifests largely depends on the pattern and strength of integration among modules. Macaques appear to have achieved a relaxed integration among modules in the cranium and mandible, respectively, to a degree sufficient to manifest transgressive segmentation.

The maxillary sinus of *M. cyclopis* is already larger than that of *M. fuscata* at birth; furthermore, the postnatal growth rate is much faster in *M. cyclopis* than in *M. fuscata*. Hybridization shifted the maxillary sinus size at birth by the proportion of ancestry, whereas the growth rate of hybrids was as fast as that of *M. cyclopis*, regardless of the proportion of ancestry. Although the genetic mechanisms that underlie the non-additive inheritance in the postnatal growth rate of the maxillary sinus are unknown, two hypotheses can be proposed. The first is that *M. fuscata*-type cytoplasmic (e.g., mitochondrial) genes restrict the growth of the sinus, which were not introduced in the

hybrids because of male-biased migration, and thus all hybrids exhibited a growth rate as fast as that of *M. cyclopis*. Maternal inheritance associated with nuclear genes, e.g., genomic imprinting, cannot explain the deviations in the second and subsequent-generation hybrids. The second is that the epistatic interaction of *M. fuscata*-type alleles restricted the growth of the sinus, which was collapsed by hybridization. Given that backcrossed individuals did not retrieve the *M. fuscata*-like slow growth rate, the epistatic interaction, if any, was controlled by not a few genes. In either case, hybridization likely collapsed a mechanism that restricts in *M. fuscata* on the growth rate of the maxillary sinus. Consequently, the adult hybrids show a mosaic pattern, i.e., the maxillary sinus is as large as that in *M. cyclopis*, although the cranium shape is almost intermediate between the two parental species.

4.3. Evolutionary background underlying the consequences of hybridization

How hybridization affects the ontogenetic trajectory probably depends on the evolutionary processes that formed the difference in genetic architecture between parental lines. This idea originates with the finding that genetic architecture sets limits on transgressive segregations (Albertson and Kocher 2005). Unlike the cranium and mandible of macaques, the fish's whole body exhibits differences in ontogenetic direction between parental lines and between these and their hybrids in multivariate allometric space (Sinama et al. 2013; Santos-Santos et al. 2021). It can be hypothesized that the fish body might be less integrated among modules and have experienced selective pressures that act differently on each module, producing changes in ontogenetic direction. In contrast, the evolutionary forces forming the interspecific differences in macaque skulls may not have been sufficiently significant to affect ontogenetic directions but set the necessary genetic architecture to cause transgressive segregation in the non-allometric components in hybrids.

The genetic distance between parental lines is a significant predictor of the expression of transgressive segregation in hybrids (Stelkens and Seehausen 2009; Stelkens et al. 2009). The evolutionary history of the group consisting of *M. cyclopis*, *M. fuscata*, and *M. mulatta* has been relatively well studied. Among the three, *M. fuscata* diverged first, followed by *M. cyclopis*, and then the Chinese and Indian lineages of *M. mulatta* diverged, with gene flow between some pairs of their ancestors (Osada et al. 2021). Although the time of divergence between *M. cyclopis* and *M. fuscata* remains controversial, the two species were probably isolated no later than 0.43 million years ago, the last time the Japanese archipelago was connected to the continent (Aimi 2002). It should be noted that the substitution rate of the *M. fuscata* lineage is much higher than the other lineages, probably due to the ancestral population bottleneck and the resulting accumulation of slightly deleterious mutations (Ito et al. 2021). *M. fuscata* is also peculiar in that it has the northernmost distribution among non-human primates, and some of its morphological features probably reflect adaptation to high-latitude environments (Antón 1996). Such relatively deep divergence and specialization in the parental lineages probably formed the genetic architecture that produced transgressive phenotypes in hybrids without changing the direction of the ontogenetic trajectory. This is in contrast to the case of pelvic morphology of hybrids between Chinese and Indian lineages of *M. mulatta*, which shows weak inter-lineage differences and no evidence of transgressive phenotypes (Buck et al. 2021). The divergence between Chinese and Indian lineages of *M. mulatta* is shallower than that between *M. cyclopis* and *M. mulatta*, but not as different. The demographic history and adaptive evolution, not just the depth of divergence, of the parental lineages is likely to be the key to what variation is manifested in hybrids.

The maxillary sinus in macaques is peculiar as the growth rate shows cytoplasmic or epistatic inheritance. If epistatic interaction restricts the growth rate of the maxillary sinus in *M. fuscata*,

then the genetic architecture could have been formed via natural selection, i.e., a co-adapted gene complex. The small maxillary sinus may be advantageous in the high-latitude environment inhabited by *M. fuscata*, because it could provide space for nasal cavity expansion or to support a strong bite. In fact, *M. fuscata* populations at higher latitudes have a larger nasal cavity and a smaller maxillary sinus (Rae et al. 2003), and *M. fuscata* shows a cranial adaptation to a high attrition diet compared to its relatives (Antón 1996). Alternatively, the maxillary sinus growth rate may be controlled by a genetic factor that pleiotropically affects an unknown functional trait because it is questionable whether the maxillary sinus has a functional role (Rae and Koppe 2004; Márquez 2008) or is related to biomechanical force (Rae and Koppe 2008). In either case, a somewhat independent trait that is under different selective pressure from the surrounding structure, such as the maxillary sinus, may result in specific ontogenetic trajectory differentiations in hybrids, whereas highly integrated traits may not.

4.3. Conclusions

This study showed that: (1) Hybridization shifts the ontogenetic trajectories of the cranium and mandible shapes in a nearly additive manner. (2) The transgressive phenotypes observed in the cranium and mandible shapes were not ascribed to the dissociations of postnatal ontogenetic directions in multivariate shape space but were likely formed by prenatal shape modifications. (3) Hybridization collapsed a mechanism found in one parental species that restricts the growth rate of the maxillary sinus, producing hybrids with a mosaic pattern, i.e., the maxillary sinus was as large as that of the opposite parental species, although the cranium shape was intermediate. This study has some limitations. First, the skeletal specimens used as surrogates for parental populations may differ in morphology from the actual parental populations because of regional intraspecific variations, although the surrogates were selected from localities as close to the hybrid population

locality as possible; this may distort the evaluation of transgression and closeness. Second, the ontogenetic trajectories lack stability because of the small sample size, and the present findings should be validated based on a larger sample size. Third, the F2, BC0, and BC1 categorized in this study may include later generations, and such genetic heterogeneity of group members may obscure patterns of variation; this concern could be addressed by inferring generations in detail based on fine-scale phased data or using the samples with known genealogy. Despite these limitations, this study highlights the complex genetic and ontogenetic bases underlying hybridization-induced differentiations in ontogenetic trajectory and the resultant morphological diversifications.

References

Ackermann, R. R., M. L. Arnold, M. D. Baiz, J. A. Cahill, L. Cortés-Ortiz, B. J. Evans, B. R. Grant, P. R. Grant, B. Hallgrimsson, R. A. Humphreys, C. J. Jolly, J. Malukiewicz, C. J. Percival, T. B. Ritzman, C. Roos, C. C. Roseman, L. Schroeder, F. H. Smith, K. A. Warren, R. K. Wayne, and D. Zinner. 2019. Hybridization in human evolution: Insights from other organisms. Evol. Anthropol. 28:189–209.

Ackermann, R. R., and J. M. Bishop. 2010. Morphological and molecular evidence reveals recent hybridization between gorilla taxa. Evolution 64:271–290.

Ackermann, R. R., L. Schroeder, J. Rogers, and J. M. Cheverud. 2014. Further evidence for phenotypic signatures of hybridization in descendant baboon populations. J. Hum. Evol. 76:54–62.

Adams, D. C., M. L. Collyer, A. Kaliontzopoulou, and E. K. Baken. 2021. Geomorph: Software for geometric morphometric analyses. R package version 4.0. https://cran.r-project.org/package=geomorph.

Aimi, M. 2002. The oldest fossil macaque from Japan. Primate Res. 18:239-245 [Japanese with English abstract].

Albertson, R. C., and T. D. Kocher. 2005. Genetic architecture sets limits on transgressive segregation in hybrid cichlid fishes. Evolution 59:686–690.

Alexander, D. H., and J. Novembre. 2009. Fast model-based estimation of ancestry in unrelated individuals. Genome Res. 19:1655–1664.

Anderson, E. C., and E. A. Thompson. 2002. A model-based method for identifying species hybrids using multilocus genetic data. Genetics 160:1217–1229.

Antón, S. C. 1996. Cranial adaptation to a high attrition diet in Japanese macaques. Int. J. Primatol. 17:401–427.

Arbour, J., and C. Brown. 2020. LOST: Missing morphometric data simulation and estimation. R package version 2.0.2. https://CRAN.R-project.org/package=LOST.

Arbour, J. H., and C. M. Brown. 2014. Incomplete specimens in geometric morphometric analyses. Methods Ecol. Evol. 5:16–26.

Arnold, M. L., and K. Kunte. 2017. Adaptive genetic exchange: A tangled history of admixture and evolutionary innovation. Trends Ecol. Evol. 32:601–611.

Baken, E. K., M. L. Collyer, A. Kaliontzopoulou, and D. C. Adams. 2021. geomorph v4.0 and gmShiny: Enhanced analytics and a new graphical interface for a comprehensive morphometric experience. Methods Ecol. Evol. 12:2355–2363.

Bastir, M., P. O'Higgins, and A. Rosas. 2007. Facial ontogeny in Neanderthals and modern humans. Proc. R. Soc. Lond. B. Biol. Sci. 274:1125–1132.

Boel, C., D. Curnoe, and Y. Hamada. 2019. Craniofacial shape and nonmetric trait variation in hybrids of the Japanese macaque (*Macaca fuscata*) and the Taiwanese macaque (*Macaca cyclopis*). Int. J. Primatol. 40:214–243.

Bolger, A. M., M. Lohse, and B. Usadel. 2014. Trimmomatic: a flexible trimmer for Illumina sequence data. Bioinformatics 30:2114–2120.

Buck, L. T., D. C. Katz, R. R. Ackermann, L. J. Hlusko, S. Kanthaswamy, and T. D. Weaver. 2021. Effects of hybridization on pelvic morphology: A macaque model. J. Hum. Evol. 159:103049.

Cheverud, J. M., S. C. Jacobs, and A. J. Moore. 1993. Genetic differences among subspecies of the saddle-back tamarin (*Saguinus fuscicollis*): evidence from hybrids. Am. J. Primatol. 31:23–39.

Collyer, M. L., and D. C. Adams. 2018. RRPP: An r package for fitting linear models to high‐dimensional data using residual randomization. Methods Ecol. Evol. 9:1772–1779.

Collyer, M. L., and D. C. Adams. 2021. RRPP: Linear model evaluation with randomized residuals in a permutation procedure. https://cran.r-project.org/web/packages/RRPP.

Corse, E., G. Neve, M. Sinama, N. Pech, C. Costedoat, R. Chappaz, and G. Andre. 2012. Plasticity of ontogenetic trajectories in cyprinids: a source of evolutionary novelties. Biol. J. Linn. Soc. Lond. 106:342–355.

Cortés-Ortiz, L., I. Agostini, L. M. Aguiar, M. Kelaita, F. E. Silva, and J. C. Bicca-Marques. 2015. Hybridization in howler monkeys: Current understanding and future directions. Pp. 107–131 *in* M. M. Kowalewski, P. A. Garber, L. Cortés-Ortiz, B. Urbani, and D. Youlatos, eds. Howler Monkeys: Adaptive Radiation, Systematics, and Morphology. Springer New York, New York.

Dryden, I. L. 2021. shapes: Statistical Shape Analysis. R package version 1.2.6. https://CRAN.R-project.org/package=shapes.

Eichel, K. A., and R. R. Ackermann. 2016. Variation in the nasal cavity of baboon hybrids with implications for late Pleistocene hominins. J. Hum. Evol. 94:134–145.

Fox, J., and S. Weisberg. 2019. An R companion to Applied Regression, Third edition. Sage, Thousand Oaks CA.

Fuzessy, L. F., I. de O. Silva, J. Malukiewicz, F. F. R. Silva, M. do C. Pônzio, V. Boere, and R. R. Ackermann. 2014. Morphological variation in wild marmosets (*Callithrix penicillata* and *C. geoffroyi*) and their hybrids. Evol. Biol. 41:480–493.

Gunz, P., S. Neubauer, B. Maureille, and J.-J. Hublin. 2010. Brain development after birth differs between Neanderthals and modern humans. Curr. Biol. 20:R921-2.

Hamada, Y., T. Mouri, Y. Kunimatsu, K. Chatani, A. Yamamoto, S. Goto, and Y. Kawamoto. 2008. Morphological study on the hybridization between Taiwanese and Japanese macaques in Wakayama Prefecture I: Relationship between tail length/the number of caudal vertebrae and hybrid index. Pp. 9–39 *in* Y. Kawamoto, ed. Effect of introduced species on biological diversity: a synthetic study on a hybrid population of Taiwanese macaques in Wakayama. Y. Kawamoto, Inuyama. [Japanese].

Hamada, Y., A. Yamamoto, Y. Kunimatsu, S. Tojima, T. Mouri, and Y. Kawamoto. 2012. Variability of tail length in hybrids of the Japanese macaque (*Macaca fuscata*) and the Taiwanese macaque (*Macaca cyclopis*). Primates 53:397–411.

Holtmeier, C. L. 2001. Heterochrony, maternal effects, and phenotypic variation among sympatric pupfishes. Evolution 55:330–338.

Ito, T. 2019. Effects of different segmentation methods on geometric morphometric data collection from primate skulls. Methods Ecol. Evol. 10:1972–1984.

Ito, T., T. Hayakawa, N. Suzuki–Hashido, Y. Hamada, Y. Kurihara, G. Hanya, A. Kaneko, T. Natsume, S. Aisu, T. Honda, S. Yachimori, T. Anezaki, T. Omi, S. Hayama, M. Tanaka, H. Wakamori, H. Imai, and Y. Kawamoto. 2021. Phylogeographic history of Japanese macaques. J. Biogeogr. 48:1420–1431.

Ito, T., Y. Kawamoto, Y. Hamada, and T. D. Nishimura. 2015. Maxillary sinus variation in hybrid macaques: Implications for the genetic basis of craniofacial pneumatization. Biol. J. Linn. Soc. Lond. 115:333–347.

Jombart, T. 2008. adegenet: a R package for the multivariate analysis of genetic markers. Bioinformatics 24:1403–1405.

Kagawa, K., and G. Takimoto. 2018. Hybridization can promote adaptive radiation by means of transgressive segregation. Ecol. Lett. 21:264–274.

Kassambara, A. 2023. rstatix: Pipe-Friendly Framework for Basic Statistical Tests. R package version 0.7.2. https://CRAN.R-project.org/package=rstatix.

Kawamoto, Y., S. Kawamoto, S. Kawai, A. Saito, H. Ohsawa, S. Goto, H. Nigi, Y. Muroyama, K. Shirai, Y. Morimitsu, and K. Suzuki. 2008a. Genetic study on the hybridization in Wakayama Prefecture. Pp. 77–132 *in* Y. Kawamoto, ed. Effect of introduced species on biological diversity: a synthetic study on a hybrid population of Taiwanese macaques in Wakayama. Y. Kawamoto, Inuyama. [Japanese].

Kawamoto, Y., H. Ohsawa, H. Nigi, T. Maruhashi, S. Maekawa, K. Shirai, and S. Araki. 2001. Genetic assessment of a hybrid population between Japanese and Taiwan macaques in Wakayama prefecture. Primate Res. 17:13-24 [Japanese with English abstract].

Kawamoto, Y., K.-I. Tomari, S. Kawai, and S. Kawamoto. 2008b. Genetics of the Shimokita macaque population suggest an ancient bottleneck. Primates 49:32–40.

Kikinis, R., S. D. Pieper, and K. G. Vosburgh. 2014. 3D Slicer: A platform for subject-specific image

analysis, visualization, and clinical support. Pp. 277–289 *in* F. A. Jolesz, ed. Intraoperative Imaging and Image-Guided Therapy. Springer New York, New York.

Langmead, B., and S. L. Salzberg. 2012. Fast gapped-read alignment with Bowtie 2. Nat. Methods 9:357–359.

Lischer, H. E. L., and L. Excoffier. 2012. PGDSpider: An automated data conversion tool for connecting population genetics and genomics programs. Bioinformatics 28:298–299.

Mallet, J. 2005. Hybridization as an invasion of the genome. Trends Ecol. Evol. 20:229–237.

Malukiewicz, J., V. Boere, L. F. Fuzessy, A. D. Grativol, J. A. French, I. de Oliveira e Silva, L. C. M. Pereira, C. R. Ruiz-Miranda, Y. M. Valença, and A. C. Stone. 2014. Hybridization effects and genetic diversity of the common and black-tufted marmoset (*Callithrix jacchus* and *Callithrix penicillata*) mitochondrial control region. Am. J. Phys. Anthropol. 155:522–536.

Márquez, S. 2008. The paranasal sinuses: the last frontier in craniofacial biology. Anat. Rec. 291:1350–1361.

Mérot, C., V. Debat, Y. Le Poul, R. M. Merrill, R. E. Naisbit, A. Tholance, C. D. Jiggins, and M. Joron. 2020. Hybridization and transgressive exploration of colour pattern and wing morphology in *Heliconius* butterflies. J. Evol. Biol. 33:942–956.

Mitteroecker, P., P. Gunz, M. Bernhard, K. Schaefer, and F. L. Bookstein. 2004. Comparison of cranial ontogenetic trajectories among great apes and humans. J. Hum. Evol. 46:679–698.

Mouri, T. 1996. Multivariate cranial ontogenetic allometries in crab-eating, rhesus and Japanese macaques. Anthropol. Sci. 104:281–303.

Mouri, T. 1994. Postnatal growth and sexual dimorphism in the skull of the Japanese macaque (*Macaca fuscata*). Anthropol. Sci. 102:43–56.

Ohsawa, H., Y. Morimitsu, Y. Kawamoto, Y. Muroyama, S. Maekawa, H. Nigi, H. Tori, S. Goto, T. Maruhashi, N. Nakagawa, J. Nakatani, T. Tanaka, S. Hayakawa, A. Yamada, S. Hayashi, H. Seino, M. Saeki, S. Kawai, H. Hagiwara, K. Suzuki, K. Suzuki, S. Uetsuki, M. Okano, T.

Okumura, A. Yoshida, and N. Yokoyama. 2005. Population explosion of Taiwanese macaques in Japan. Nat. Hist. J Chulalongkorn Univ. Supplement 1:55–60.

Osada, N., K. Matsudaira, Y. Hamada, and S. Malaivijitnond. 2021. Testing sex-biased admixture origin of macaque species using autosomal and X-chromosomal genomic sequences. Genome Biol. Evol. 13:1–14.

Peterson, B. K., J. N. Weber, E. H. Kay, H. S. Fisher, and H. E. Hoekstra. 2012. Double digest RADseq: An inexpensive method for de novo SNP discovery and genotyping in model and non-model species. PLoS One 7:e37135.

Ponce de León, M. S., and C. P. Zollikofer. 2001. Neanderthal cranial ontogeny and its implications for late hominid diversity. Nature 412:534–538.

Purcell, S., B. Neale, K. Todd-Brown, L. Thomas, M. A. R. Ferreira, D. Bender, J. Maller, P. Sklar, P. I. W. de Bakker, M. J. Daly, and P. C. Sham. 2007. PLINK: A tool set for whole-genome association and population-based linkage analyses. Am. J. Hum. Genet. 81:559–575.

R Developmental Core Team. 2021. R: A language and environment for statistical computing. Vienna.

Rae, T. C., R. A. Hill, Y. Hamada, and T. Koppe. 2003. Clinal variation of maxillary sinus volume in Japanese macaques (*Macaca fuscata*). Am. J. Primatol. 59:153–158.

Rae, T. C., and T. Koppe. 2004. Holes in the head: Evolutionary interpretations of the paranasal sinuses in catarrhines. Evol. Anthropol. 13:211–223.

Rae, T. C., and T. Koppe. 2008. Independence of biomechanical forces and craniofacial pneumatization in *Cebus*. Anat. Rec. 291:1414–1419.

Renaud, S., P. Alibert, and J.-C. Auffray. 2012. Modularity as a source of new morphological variation in the mandible of hybrid mice. BMC Evol. Biol. 12:141.

Rieseberg, L. H., M. A. Archer, and R. K. Wayne. 1999. Transgressive segregation, adaptation and speciation. Heredity 83:363–372.

Rochette, N. C., and J. M. Catchen. 2017. Deriving genotypes from RAD-seq short-read data using Stacks. Nat. Protoc. 12:2640–2659.

Rogers, J., M. Raveendran, R. A. Harris, T. Mailund, K. Leppälä, G. Athanasiadis, M. H. Schierup, J. Cheng, K. Munch, J. A. Walker, and Others. 2019. The comparative genomics and complex population history of *Papio* baboons. Sci. Adv. 5:eaau6947.

Roos, C., D. Zinner, L. S. Kubatko, C. Schwarz, M. Yang, D. Meyer, S. D. Nash, J. Xing, M. A. Batzer, M. Brameier, F. H. Leendertz, T. Ziegler, D. Perwitasari-Farajallah, T. Nadler, L. Walter, and M. Osterholz. 2011. Nuclear versus mitochondrial DNA: evidence for hybridization in colobine monkeys. BMC Evol. Biol. 11:77.

Sakaguchi, S., K. Horie, N. Ishikawa, A. J. Nagano, M. Yasugi, H. Kudoh, and M. Ito. 2017. Simultaneous evaluation of the effects of geographic, environmental and temporal isolation in ecotypic populations of Solidago virgaurea. New Phytol. 216:1268–1280.

Sakaguchi, S., T. Sugino, Y. Tsumura, M. Ito, M. D. Crisp, D. M. J. S. Bowman, A. J. Nagano, M. N. Honjo, M. Yasugi, H. Kudoh, Y. Matsuki, Y. Suyama, and Y. Isagi. 2015. High-throughput linkage mapping of Australian white cypress pine (*Callitris glaucophylla*) and map transferability to related species. Tree Genet. Genomes 11:1–12.

Santos-Santos, J. H., L. Audenaert, E. Verheyen, and D. Adriaens. 2021. Ontogenetic divergence generates novel phenotypes in hybrid cichlids. J. Anat. 238:1116–1127.

Schillaci, M. A., J. W. Froehlich, J. Supriatna, L. Jones-Engel, and L. Jones Engel. 2005. The effects of hybridization on growth allometry and craniofacial form in Sulawesi macaques. J. Hum. Evol. 49:335–369.

Schlager, S. 2017. Morpho and Rvcg - Shape Analysis in R. Pp. 217–256 *in* G. Zheng, S. Li, and G. Szekely, eds. Statistical Shape and Deformation Analysis: Methods, Implementation and Applications. Academic Press, San Diego.

Seehausen, O. 2004. Hybridization and adaptive radiation. Trends Ecol. Evol. 19:198–207.

Shirai, K., Y. Kawamoto, and Y. Morimitsu. 2018. Wakayama Taiwanese macaque “report of troop eradication” and Chiba rhesus macaque problem “current status and issues.” Primate Res. 34:15 [Japanese].

Simons, E. A., and S. R. Frost. 2021. Ontogenetic allometry and scaling in catarrhine crania. J. Anat. 238:693–710.

Sinama, M., A. Gilles, C. Costedoat, E. Corse, J.-M. Olivier, R. Chappaz, and N. Pech. 2013. Non-homogeneous combination of two porous genomes induces complex body shape trajectories in cyprinid hybrids. Front. Zool. 10:22.

Singleton, M. 2012. Postnatal cranial development in papionin primates: An alternative model for hominin evolutionary development. Evol. Biol. 39:499–520.

Smith, D. G., and L. M. Scott. 1989. Heterosis associated with regional crossbreeding between captive groups of rhesus macaques. Am. J. Primatol. 19:255–260.

Stelkens, R. B., C. Schmid, O. Selz, and O. Seehausen. 2009. Phenotypic novelty in experimental hybrids is predicted by the genetic distance between species of cichlid fish. BMC Evol. Biol. 9:283.

Stelkens, R., and O. Seehausen. 2009. Genetic distance between species predicts novel trait expression in their hybrids. Evolution 63:884–897.

Suzuki-Hashido, N., T. Hayakawa, A. Matsui, Y. Go, Y. Ishimaru, T. Misaka, K. Abe, H. Hirai, Y. Satta, and H. Imai. 2015. Rapid expansion of phenylthiocarbamide non-tasters among Japanese macaques. PLoS One 10:1–21.

Svardal, H., A. J. Jasinska, C. Apetrei, G. Coppola, Y. Huang, C. A. Schmitt, B. Jacquelin, V. Ramensky, M. Müller-Trutwin, M. Antonio, G. Weinstock, J. P. Grobler, K. Dewar, R. K. Wilson, T. R. Turner, W. C. Warren, N. B. Freimer, and M. Nordborg. 2017. Ancient hybridization and strong adaptation to viruses across African vervet monkey populations. Nat. Genet. 49:1705–1713.

Taylor, N. D., and M. A. Schillaci. 2008. Heterochrony in hybrid macaques. Zool. Stud. 47:713–719.

Taylor, S. A., and E. L. Larson. 2019. Insights from genomes into the evolutionary importance and prevalence of hybridization in nature. Nat Ecol Evol 3:170–177.

Thompson, K. A., M. Urquhart-Cronish, K. D. Whitney, L. H. Rieseberg, and D. Schluter. 2021. Patterns, Predictors, and Consequences of Dominance in Hybrids. Am. Nat. 197:E72–E88.

Toyoda, N., T. Ito, T. Sato, and T. Nishimura. 2022. Ontogenetic differences in mandibular morphology

of two related macaque species and its adaptive implications. Anat. Rec. 305:3430–3440.

Vioarsdóttir, U. S., and S. Cobb. 2004. Inter- and intra-specific variation in the ontogeny of the hominoid facial skeleton: testing assumptions of ontogenetic variability. Ann. Anat. 186:423–428.

Warton, D. I., R. A. Duursma, D. S. Falster, and S. Taskinen. 2012. smatr 3–an R package for estimation and inference about allometric lines. Methods Ecol. Evol. 3:257–259.

Wringe, B. F., R. R. E. Stanley, N. W. Jeffery, E. C. Anderson, and I. R. Bradbury. 2017. parallelnewhybrid: an R package for the parallelization of hybrid detection using newhybrids. Mol. Ecol. Resour. 17:91–95.

Tables

Table 1. Multivariate regression of shape on lnCS, hybrid class and their interactions. Each sex was analyzed separately.

Response	Source	*Df*	*SS*	*MS*	R^2	*F*	*Z*	*P*
Female								
cranium	lnCS	1	0.474	0.474	0.522	290.1	3.8	0.001
	hybrid class	5	0.084	0.017	0.092	10.3	7.0	0.001
	lnCS:hybrid class	5	0.010	0.002	0.011	1.2	1.4	0.074
	residuals	134	0.219	0.002	0.241			
	total	145	0.909					
mandible	lnCS	1	0.433	0.433	0.494	263.8	4.0	0.001
	hybrid class	5	0.097	0.019	0.110	11.8	7.6	0.001
	lnCS:hybrid class	5	0.012	0.002	0.013	1.4	2.2	0.015
	residuals	133	0.218	0.002	0.249			
	total	144	0.877					
Male								
cranium	lnCS	1	0.691	0.691	0.659	414.9	3.4	0.001
	hybrid class	5	0.059	0.012	0.056	7.1	7.6	0.001
	lnCS:hybrid class	5	0.012	0.002	0.011	1.4	2.5	0.011
	residuals	126	0.21	0.002	0.200			
	total	137	1.05					
mandible	lnCS	1	0.582	0.582	0.614	319.9	3.7	0.001
	hybrid class	5	0.067	0.013	0.070	7.3	8.0	0.001
	lnCS:hybrid class	5	0.012	0.002	0.012	1.3	1.6	0.053
	residuals	124	0.226	0.002	0.238			
	total	135	0.947					

Type II sum of squares was used.

Table 2. Pairwise vector correlations in the multivariate regression of shape against lnCS, hybrid class, and their interactions. The upper triangle indicates the angle (radians) and the lower triangle indicates the *P*-value.

		cyclopis_P0	BC0	F1	F2	BC1	fuscata
Female							
cranium	cyclopis_P0		0.244	0.404	0.308	0.269	0.278
	BC0	0.507		0.478	0.214	0.199	0.188
	F1	0.934	0.61		0.511	0.445	0.488
	F2	0.05	0.24	0.501		0.224	0.206
	BC1	0.135	0.239	0.705	0.028		0.171
	fuscata	0.056	0.225	0.534	0.026	0.071	
mandible	cyclopis_P0		0.229	0.677	0.326	0.317	0.313
	BC0	0.83		0.575	0.185	0.195	0.228
	F1	0.106	0.231		0.607	0.621	0.635
	F2	0.157	0.693	0.167		0.19	0.287
	BC1	0.109	0.367	0.13	0.346		0.209
	fuscata	0.095	0.067	0.109	0.004	0.015	
Male							
cranium	cyclopis_P0		0.163	0.283	0.221	0.188	0.212
	BC0	0.353		0.316	0.183	0.173	0.169
	F1	0.92	0.748		0.374	0.264	0.308
	F2	0.033	0.095	0.421		0.243	0.229
	BC1	0.154	0.132	0.965	0.001		0.187
	fuscata	0.006	0.027	0.774	0.003	0.018	
mandible	cyclopis_P0		0.167	0.382	0.192	0.144	0.17
	BC0	0.523		0.417	0.197	0.182	0.226
	F1	0.499	0.297		0.507	0.362	0.344
	F2	0.382	0.189	0.073		0.226	0.265
	BC1	0.839	0.25	0.573	0.062		0.17
	fuscata	0.345	0.004	0.633	0.003	0.222	

Table 3. Regression of lnCS and bgPC1 on the hybrid index in the admixed adult samples. Deviations of elevation and slope from additivity (the line passing through the means of each parent) were evaluated. Each sex was analyzed separately.

		Model fit		Slope test		Elevation test	
	Variable	R^2	*P*	*b*	*P*	*a*	*P*
Female							
cranium	lnCS	0.37	0.001	0.12	0.436	5.58	0.502
	bgPC1	0.37	0.001	-0.04	0.771	0.01	0.156
mandible	lnCS	0.43	<0.001	0.18	0.105	5.22	0.992
	bgPC1	0.6	<0.001	-0.06	0.557	0.03	0.583
maxillary sinus	lnCS	0.02	0.542	-0.11	0.022	3.33	0.086
	log ratio	0.09	0.152	-0.23	0.015	-2.25	0.071
Male							
cranium	lnCS	0.69	<0.001	0.14	0.191	5.67	0.902
	bgPC1	0.62	<0.001	-0.06	0.372	0.04	0.803
mandible	lnCS	0.61	<0.001	0.17	0.198	5.34	0.885
	bgPC1	0.59	<0.001	-0.06	0.803	0.04	0.677
maxillary sinus	lnCS	0.2	0.098	0.26	<0.001	3.22	0.216
	log ratio	0.05	0.438	0.11	<0.001	-2.45	0.194

Maxillary sinus log ratio indicates lnCS (sinus) - lnCS (cranium).

Table 4. Transgressive segregation in multivariate shape space (but univariate size for maxillary sinus) represented by Bias and Mismatch in adult samples. Bias indicates the position of the data projected on the interspecific axis, where *M. cyclopis* is zero and *M. fuscata* is one. Mismatch indicates orthogonal deviations from the interspecific axis standardized by the interspecific distance.

	BC0		F1		BC1	
	Female	Male	Female	Male	Female	Male
hybrid index	0.21	0.29	0.50	0.49	0.77	0.78
Bias						
cranium	0.30	0.36	0.74	0.72	0.77	1.01
mandible	0.18	0.33	0.51	0.30	0.77	0.81
maxillary sinus	−0.05	0.16	−0.24	0.07	0.24	0.03
Mismatch						
cranium	0.56	0.48	0.82	0.60	0.53	0.55
mandible	0.34	0.62	0.58	0.49	0.53	0.51

Figures

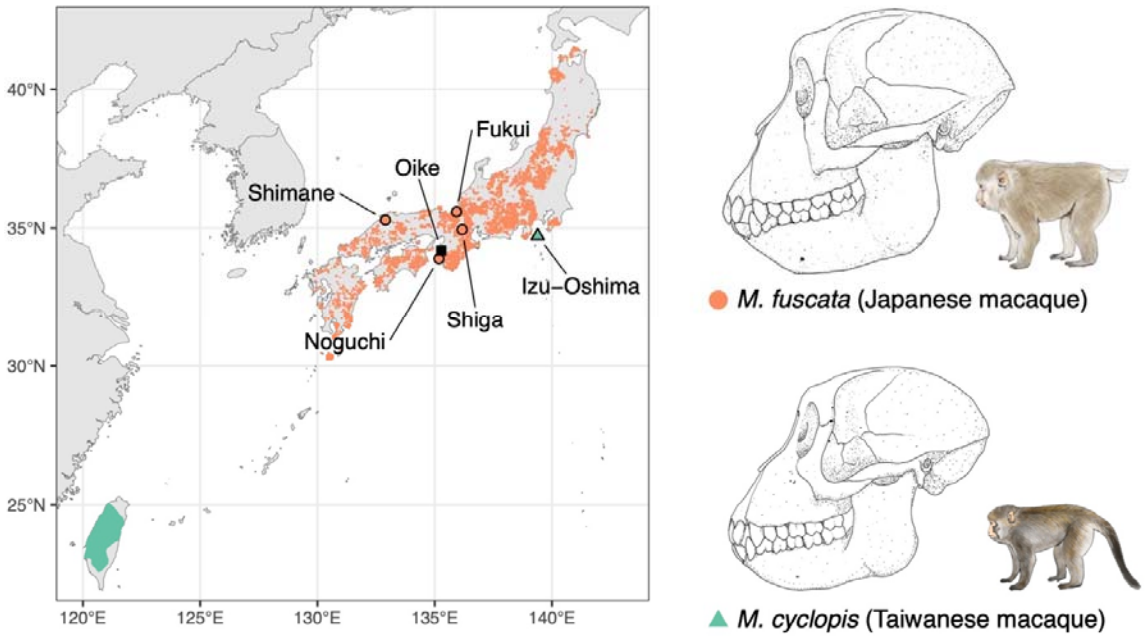

Figure 1: Natural distribution of *Macaca cyclopis* (Taiwanese macaques; blue) and *M. fuscata* (Japanese macaques; magenta) and sampling sites. Oike is the location of the hybrid population. *M. fuscata* skeletal specimens are from Fukui (*N* = 15), Shimane (*N* = 21), Shiga (*N* = 49), and Noguchi (*N* = 1). *M. cyclopis* skeletal specimens are from Izu-Oshima Island (*N* = 20), where the introduced *M. cyclopis* is distributed. This map was created by the authors using IUCN Red List Data (version 3, May 2017) and distribution surveys of Japanese animals (mammals) by the Biodiversity Center of Japan, Nature Conservation Bureau, Ministry of the Environment.

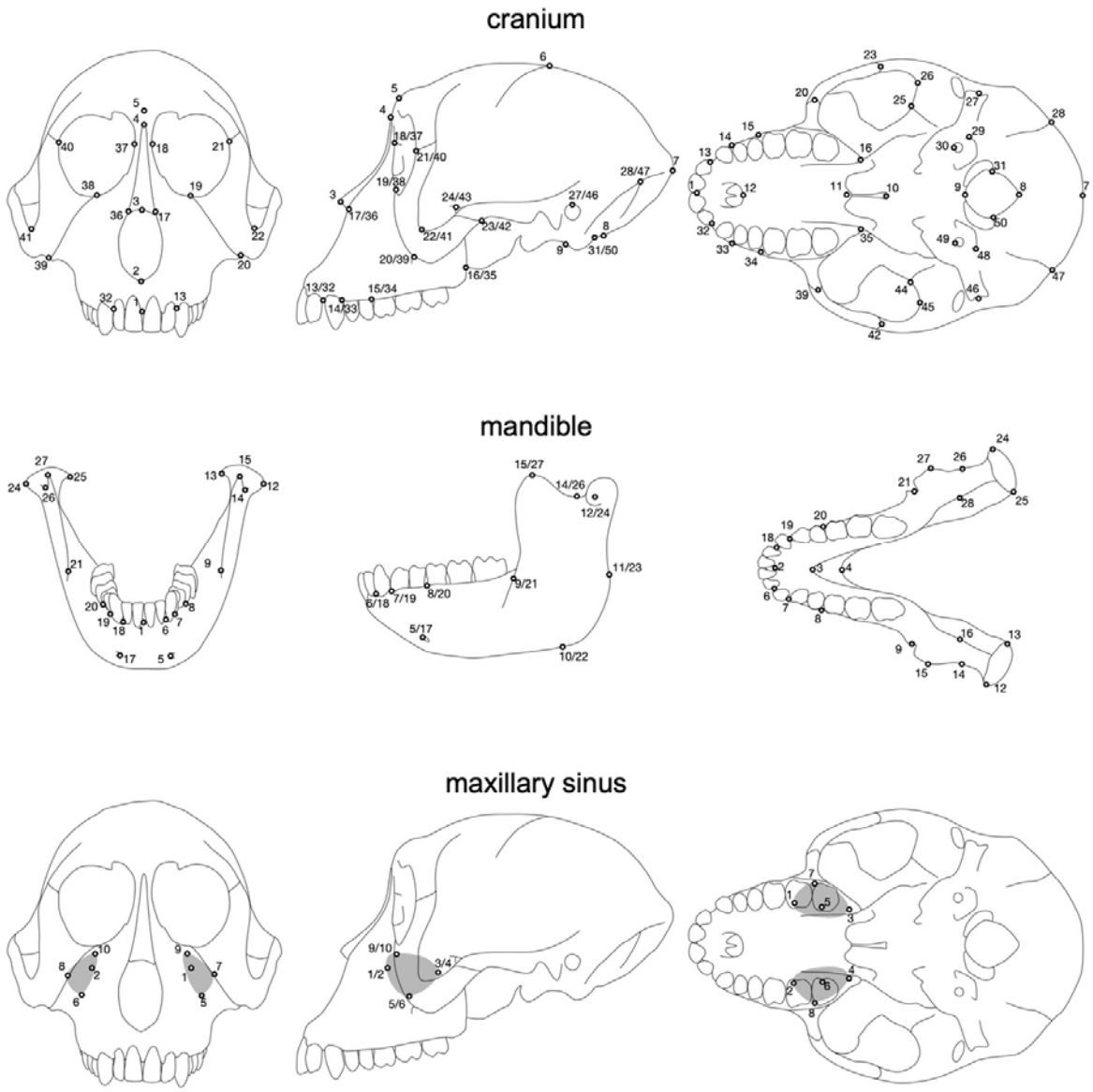

Figure 2: Landmarks used in this study.

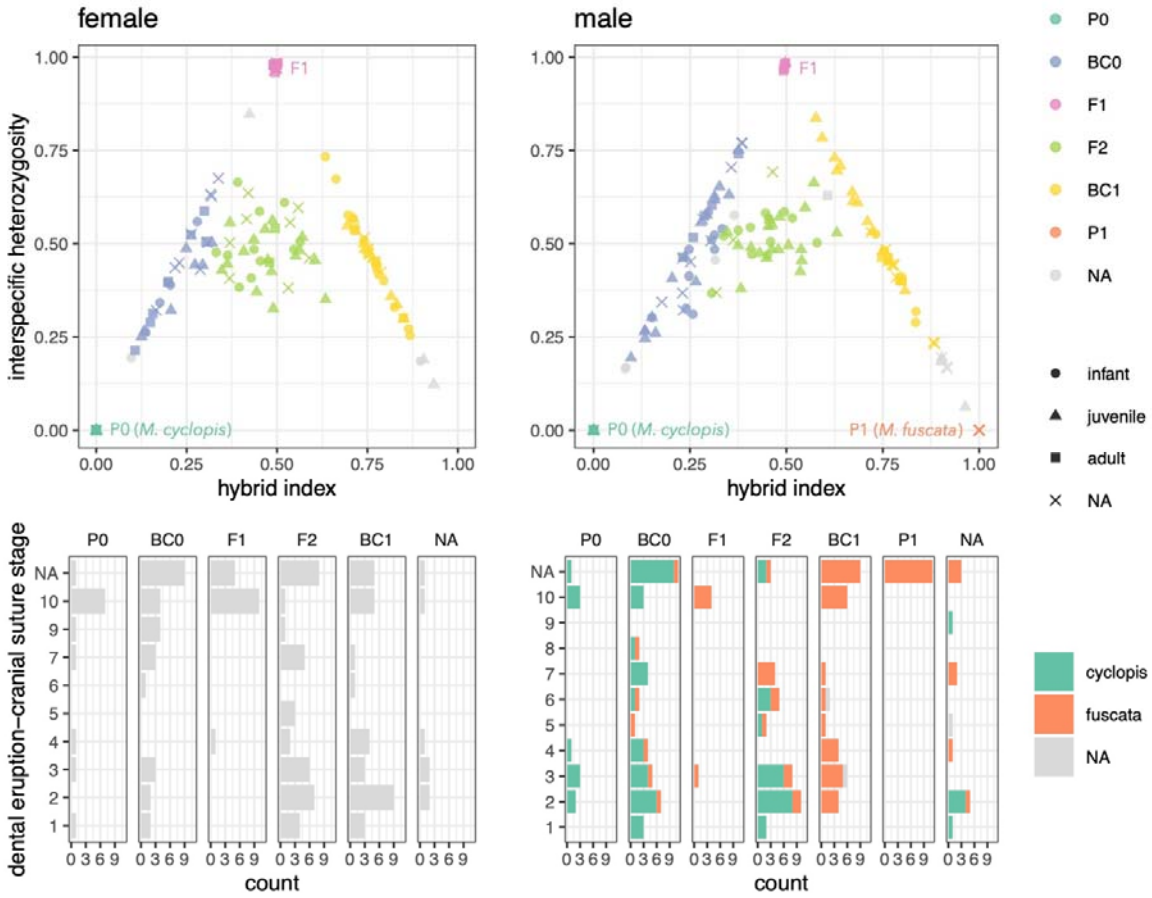

Figure 3: Population structure of the Oike population. Upper panels show the relationship between hybrid index and interspecific heterozygosity, where each individual is colored by hybrid class. Lower panels show the age structures; males are colored by Y chromosome ancestry.

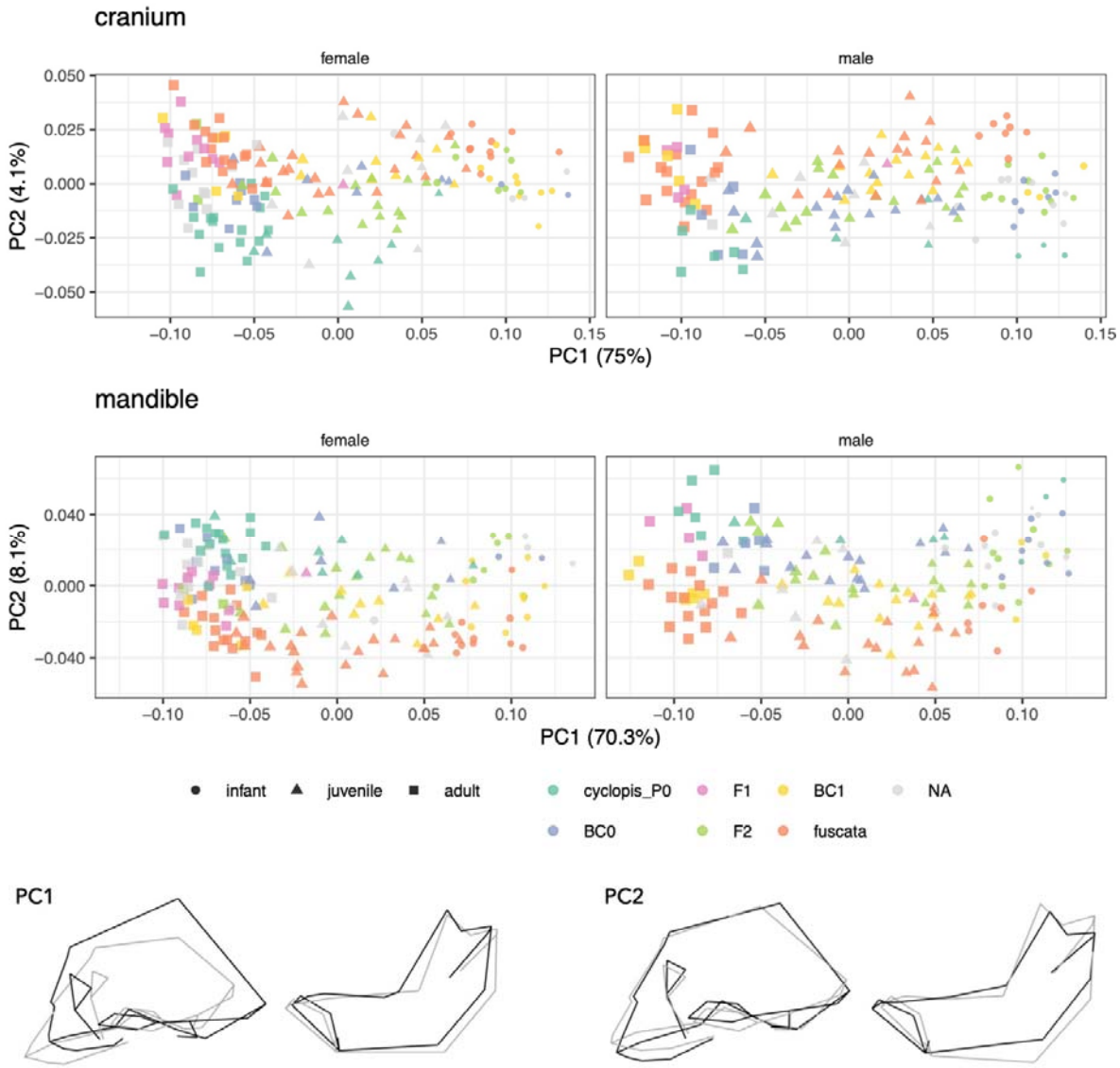

Figure 4: Variations of cranium and mandible shape represented by the first two principal components (PCs). All samples were analyzed together, but each sex was plotted separately for better visualization. Points are scaled according to lnCS. Shape changes along PC1 and PC2 are represented by wireframes (black, positive extreme; gray, negative).

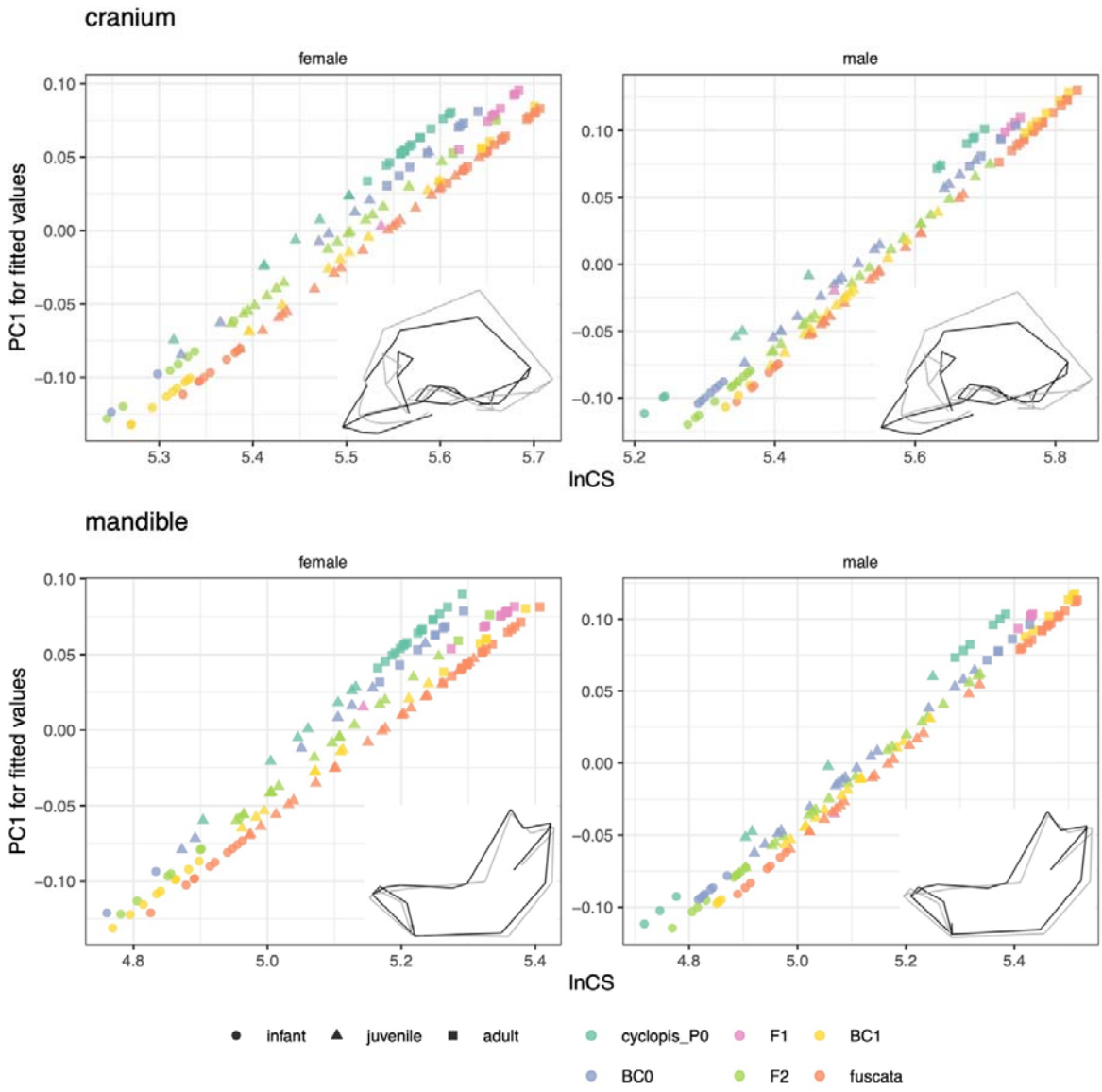

Figure 5: Ontogenetic allometry of cranial and mandibular shape represented by multivariate regression of shape against lnCS, hybrid class, and their interactions. Each sex was analyzed separately. Shape changes along PC1 for the fitted value are represented by wireframes (black, positive extreme; gray, negative).

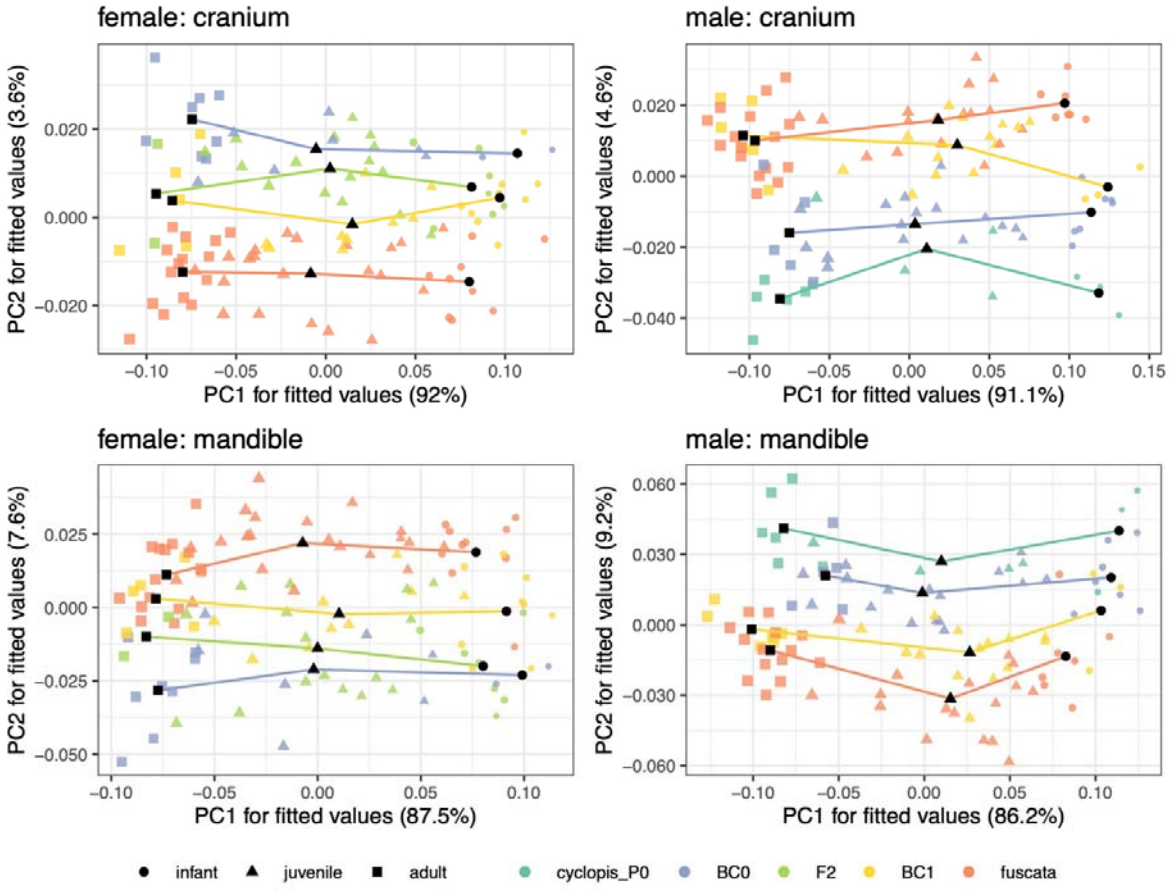

Figure 6: Ontogenetic trajectories of cranial and mandibular shape represented by the phenotypic trajectory analysis, where explanatory variables were lnCS, hybrid class, and their interactions. Each sex was analyzed separately. Hybrid classes with few samples (*M. cyclopis* and F1 for females; F1 and F2 for males) were excluded from the analyses. Points are scaled according to lnCS.

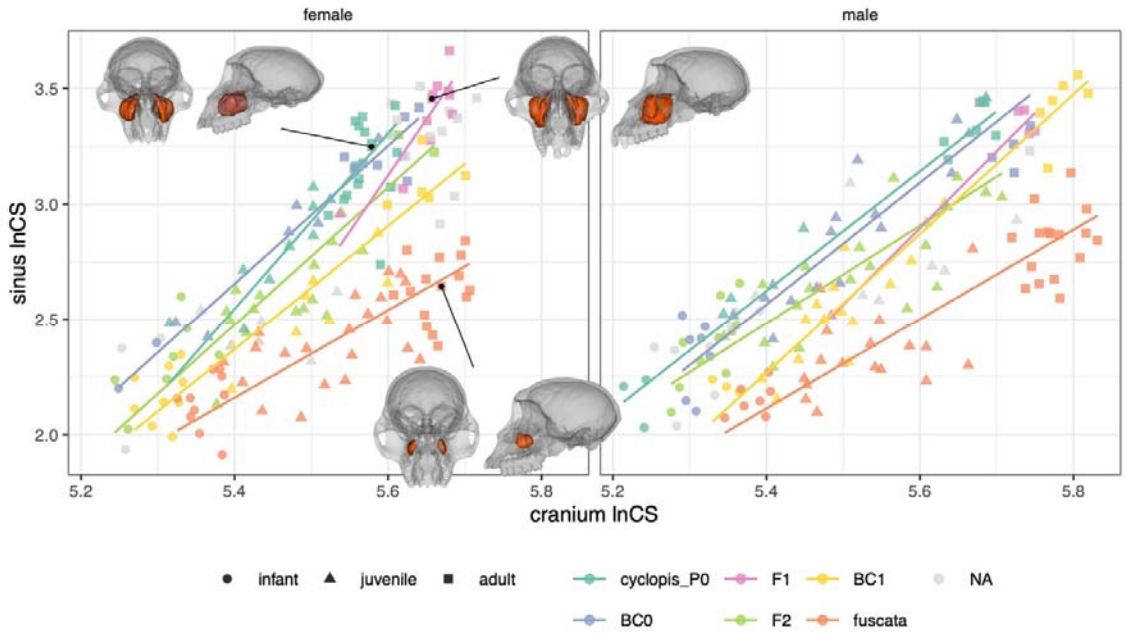

Figure 7: Ontogenetic allometry of maxillary sinus size versus the cranial size. The lines indicate the reduced major axis regression. The maxillary sinus is colored red in the transparent cranium.

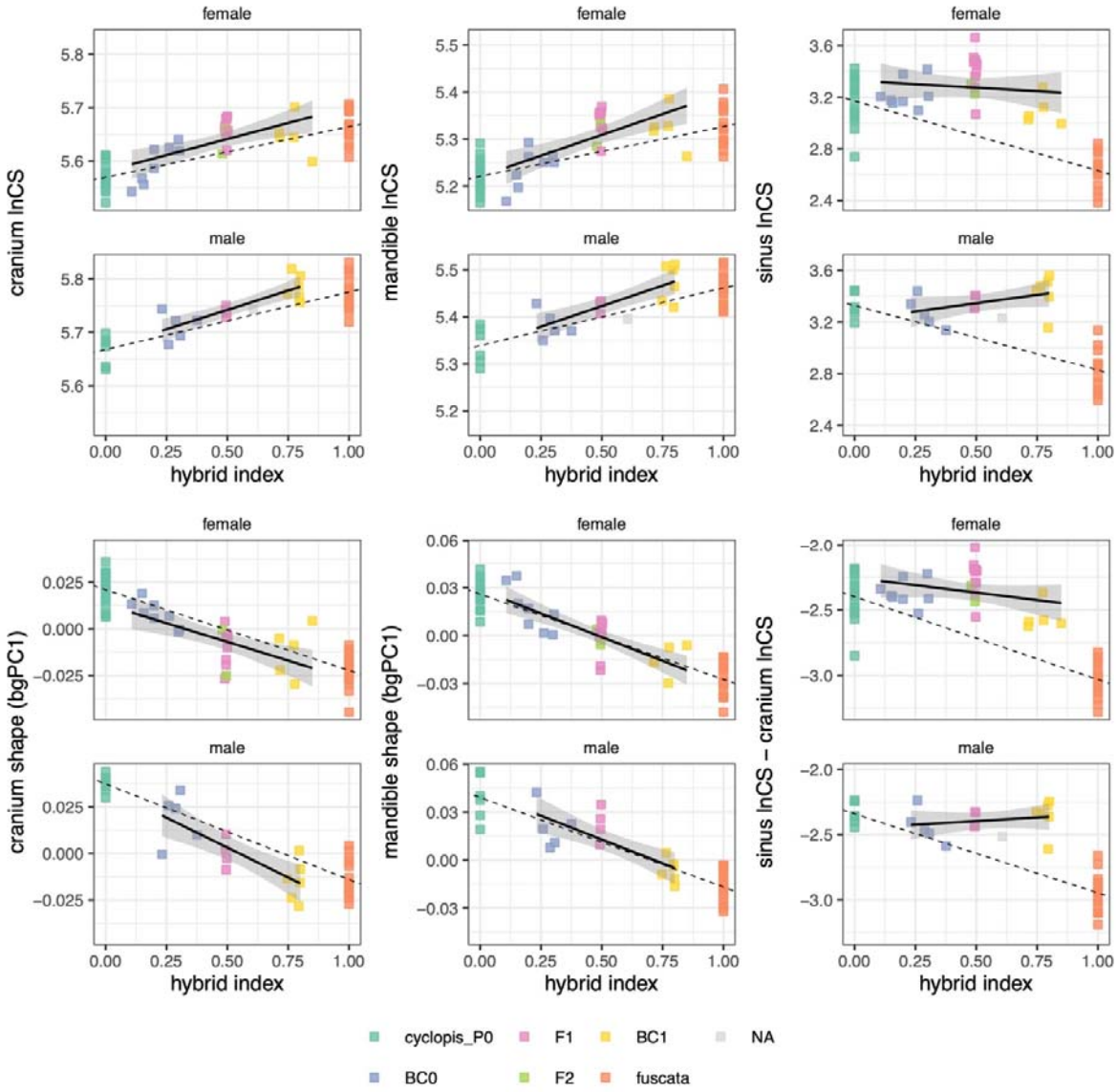

Figure 8: Relationship between morphological variation and hybrid index in adult samples. *M. fuscata* from the other populations and *M. cyclopis* are placed as 1 and 0 on the hybrid index, respectively. Dashed lines indicate the expectations of the additive model, which pass through the means of the *M. cyclopis* (P0 and the other *M. cyclopis*) and *M. fuscata* populations. Solid lines indicate the ordinary least squares regression for

the admixed individuals of the Oike population. For shape, between-group PCA (bgPCA) was performed to detect shape differences between pure *M. cyclopis* and *M. fuscata*, and admixed individuals were projected onto the bgPC1 axis.